# Multi-frequency vortex-induced vibrations of a long tensioned beam in linear and exponential shear flows

Rémi Bourguet, George E. Karniadakis, Michael S. Triantafyllou

# Multi-frequency vortex-induced vibrations of a long tensioned beam in linear and exponential shear flows

Rémi Bourguet [a,*], George Em Karniadakis [b], Michael S. Triantafyllou [c]

[a] Institut de Mécanique des Fluides de Toulouse, Université de Toulouse and CNRS, 31400 Toulouse, France
[b] Division of Applied Mathematics, Brown University, Providence, RI 02912, USA
[c] Department of Mechanical Engineering, Massachusetts Institute of Technology, Cambridge, MA 02139, USA

*Keywords:*
Vortex-induced vibrations
Narrowband and broadband multi-frequency responses
Lock-in in shear flow
Tensioned beam
Direct numerical simulation

A B S T R A C T

The multi-frequency vortex-induced vibrations of a cylindrical tensioned beam of aspect ratio 200, free to move in the in-line and cross-flow directions within first a linearly and then an exponentially sheared current are investigated by means of direct numerical simulation, at a Reynolds number equal to 330. The shape of the inflow profile impacts the spectral content of the mixed standing-traveling wave structural responses: narrowband vibrations are excited within the lock-in area, which is limited to a single region lying in the high flow velocity zone, for the linear shear case; in contrast, the lock-in condition occurs at several spanwise locations in the exponential shear case, resulting in broadband responses, containing a wide range of excited frequencies and spatial wavenumbers. The broadband in-line and cross-flow vibrations occurring for the exponential shear current have a phase difference that lies within a specific range along the entire span; this differs from the phase drift noted for narrowband responses in linear shear flow. Lower vibration amplitudes, time-averaged and fluctuating in-line force coefficients are observed for the exponential shear current. The cross-flow force coefficient has comparable magnitude for both inflow profiles along the span, except in zones where the broadband vibrations are under the lock-in condition but not the narrowband ones. As in the narrowband case, the fluid forces associated with the broadband responses are dominated by high frequencies related to high-wavenumber vibration components. Considerable variability of the effective added mass coefficients along the span is noted in both cases.

## 1. Introduction

Slender flexible cylindrical bodies placed in cross-flow exhibit vortex-induced vibrations (VIV). This phenomenon represents a canonical problem for the investigation of distributed fluid–structure interactions. The resulting oscillations have also important practical implications, especially in offshore engineering, where they cause increased fatigue damage of marine cables and risers exposed to ocean currents. The present work focuses on the multi-frequency VIV that may occur when a tensioned beam is immersed in a sheared cross-flow.

A central mechanism of VIV is first the excitation of structural vibrations due to the flow instability, and then the synchronization between the structural vibrations and the vortical patterns forming in the wake of the structure. This state

* Corresponding author.
*E-mail addresses:* bourguet@imft.fr, bourguet@mit.edu (R. Bourguet).

of wake-body frequency synchronization, referred to as lock-in condition, has been principally studied through the simpler problem of a short-span rigid cylinder vibrating within a uniform current (Bearman, 1984, 2011; Prasanth and Mittal, 2008; Sarpkaya, 2004; Singh and Mittal, 2005; Williamson and Govardhan, 2004). In this context, large amplitude oscillations of the body appear over a range of inflow velocities under the lock-in condition, which can be established at a frequency that shifts away from both the natural frequency of the structure and the Strouhal frequency, viz. the frequency of vortex shedding downstream of a stationary cylinder.

A long flexible cylinder presents an infinite set of natural frequencies; hence, when such body is immersed in a sheared current, the lock-in condition can potentially appear at several spanwise locations, resulting in structural vibrations involving multiple frequencies and structural wavenumbers. Previous studies have provided detailed descriptions of the typical responses of long flexible cylinders in uniform and non-uniform currents (Chaplin et al., 2005; Huera-Huarte and Bearman, 2009; Lie and Kaasen, 2006; Trim et al., 2005; Vandiver et al., 2009). Within shear flow, both mono- and multi-frequency VIV have been observed (e.g. Bourguet et al., 2011b, 2012; Vandiver et al., 1996; Lucor et al., 2001). Comparison of the responses of a long tensioned beam immersed in linear shear flow and exponentially sheared current, which constitutes a more realistic flow profile with respect to ocean engineering applications, has shown that multi-frequency VIV can occur for both types of currents, but a wider range of frequencies may be excited in the latter case (Lucor et al., 2006). Previous work was based on low-resolution simulations where the cylinder was constrained to oscillate in the cross-flow direction, and mainly focused on the quantification of the beam vibrations; as a consequence the impact of the shape of the shear profile on the properties of the coupled fluid–structure system remains to be clarified.

Through high-resolution simulations, the present study aims at investigating and comparing the multi-frequency VIV of a long flexible cylinder immersed in linear and exponential shear flows, with an emphasis on the changes induced in the lock-in phenomenon and fluid forces by the alteration of the current profile. The analysis is based on direct numerical simulations of the flow past a cylindrical tensioned beam of length to diameter aspect ratio 200 and free to move in the in-line and cross-flow directions, at a Reynolds number equal to 330, based on the maximum inflow velocity.

The paper is organized as follows. The physical model and the numerical method are presented in Section 2. The structural vibrations observed in both shear flow cases are described in Section 3. The impact of the inflow profile on the occurrence of the lock-in condition is analyzed in Section 4. The fluid forces are examined in Section 5. The main findings of the present work are summarized in Section 6.

## 2. Fluid–structure model and numerical method

The flow past a flexible cylinder of circular cross-section is predicted using direct numerical simulation of the three-dimensional incompressible Navier–Stokes equations. The cylinder is exposed to a current which is parallel to the global $x$-axis and sheared along the global $z$-axis. The linear and exponential inflow velocity profiles considered are similar to those employed in Lucor et al. (2006), where multi-frequency VIV characterized by distinct response bandwidth have been reported for each profile. The two velocity profiles are plotted in Fig. 1(a) and (b). In both cases, the ratio between the maximum and minimum inflow velocities is set to 3.67. In the following, all physical variables are non-dimensionalized using the cylinder diameter $D$ and the maximum inflow velocity $U$, which occurs at $z=0$. The Reynolds number (Re) based on $D$ and $U$ is equal to 330. This value was chosen in reference to a previous study concerning mono-frequency and narrowband multi-frequency responses in shear flow (Bourguet et al., 2012). Although the Reynolds number is low compared to full-scale applications, experimental studies (e.g. Dahl et al., 2010; Lie and Kaasen, 2006; Trim et al., 2005; Vandiver et al., 2009) have provided evidence that important features of the VIV analyzed here, such as the occurrence of broadband responses and the preferential in-line/cross-flow motion synchronization patterns, are also observed at high Reynolds numbers.

The cylinder aspect ratio is $L/D=200$, where $L$ is the cylinder length in its equilibrium position in quiescent fluid. It is pinned at both ends and free to move in the in-line ($x$) and cross-flow ($y$) directions. The cylinder mass ratio, defined as $m=\rho_c/\rho_f D^2$, where $\rho_c$ is its mass per unit length and $\rho_f$ the fluid density, is equal to 6. The constant tension, bending stiffness and damping of the structure are designated by $T$, $EI$ and $K$, respectively. The in-line and cross-flow displacements of the cylinder are denoted by $\zeta_x$ and $\zeta_y$. The sectional in-line and cross-flow force coefficients are defined as $C_x=2F_x/\rho_f DU^2$ and $C_y=2F_y/\rho_f DU^2$, where $F_x$ and $F_y$ are the in-line and cross-flow dimensional sectional fluid forces. The structural dynamics are governed by a tensioned beam model, expressed as follows in non-dimensional formulation (Evangelinos and Karniadakis, 1999):

$$\frac{\partial^2\boldsymbol{\zeta}}{\partial t^2}-\omega_c^2\frac{\partial^2\boldsymbol{\zeta}}{\partial z^2}+\omega_b^2\frac{\partial^4\boldsymbol{\zeta}}{\partial z^4}+\frac{K}{m}\frac{\partial\boldsymbol{\zeta}}{\partial t}=\frac{1}{2}\frac{\boldsymbol{C}}{m}, \tag{1}$$

where $\boldsymbol{\zeta}=[\zeta_x,\zeta_y]^T$ and $\boldsymbol{C}=[C_x,C_y]^T$. $t$ denotes the non-dimensional time variable. $\omega_c$ and $\omega_b$, the cable and beam phase velocities defined as $\omega_c^2=T/m$ and $\omega_b^2=EI/m$, are set to similar values in both cases, $(\omega_c,\omega_b)=(4.55,9.09)$ in the linear profile case and $(\omega_c,\omega_b)=(5,10)$ in the exponential profile case. The structural damping is set equal to zero ($K=0$) to allow maximum amplitude oscillations. As shown in the following, these parameters lead to vibrations involving high structural wavenumbers, which are representative of configurations encountered in the context of ocean engineering (Lie and Kaasen, 2006; Vandiver et al., 2009).

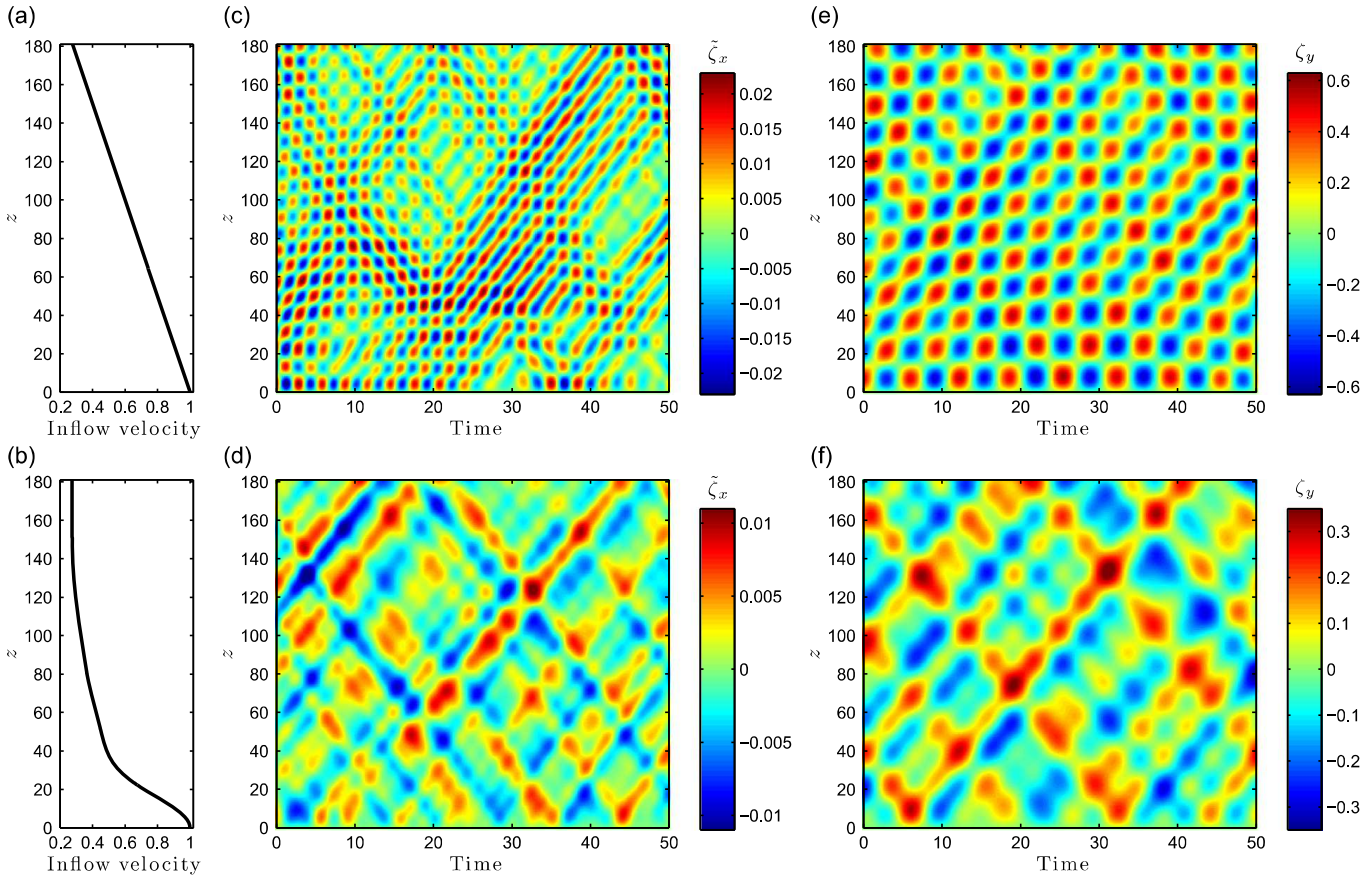


**Fig. 1.** (a) Linear and (b) exponential inflow velocity profiles and selected time series of the (c, d) in-line displacement fluctuation and (e, f) cross-flow displacement, along the span, for the (c, e) linear and (d, f) exponential inflow profiles.

The coupled fluid–structure system is solved by the parallelized code *Nektar*, based on the spectral/*hp* element method (Karniadakis and Sherwin, 1999). Details concerning validation of the numerical method have been reported in Newman and Karniadakis (1997) and Evangelinos and Karniadakis (1999). The computational domain and discretization are the same as in Bourguet et al. (2011b). The Fourier expansion used in the $z$ direction implies spanwise periodicity of the inflow velocity profile. Following a technique validated in the above mentioned reference, a buffer region (not presented in the following) is used to enforce the periodicity condition. The present analysis is based on time series of more than 300 time units, collected after convergence of the time-averaged in-line displacement of the cylinder, for each inflow velocity profile.

## 3. Vibrational responses in linear and exponential shear flows

Selected time series of the cylinder in-line and cross-flow displacements along the span, in the cases of linear and exponential inflow profiles, are presented in Fig. 1(c)–(f). In these plots, the deviation of the in-line response from its time-averaged value, $\tilde{\zeta}_x$, is considered. In both cases, the vibrations are mixtures of standing and traveling wave patterns. The amplitudes of oscillation in the case of exponential profile are substantially lower than in the linear profile case, as can be noticed in the maximum and root mean square (RMS) values of the displacements plotted in Fig. 2. The cross-flow response amplitudes and the amplitude ratio of approximately 2 between the linear and exponential profile cases are in agreement with the observations of Lucor et al. (2006) concerning VIV in the cross-flow direction only, within similar sheared currents. The change in the nature of the structural responses when the inflow profile is modified, which can be observed qualitatively in Fig. 1(c)–(f), is investigated in the following by means of spectral analysis.

The spanwise evolution of the cross-flow displacement temporal power spectral density (PSD) is plotted in Fig. 3, for both inflow velocity profiles. Both cases exhibit vibrations at multiple frequencies but the structural responses differ in the width of the excited frequency band: three main frequencies are excited along the span within a narrow band in the linear profile case, while a broadband response is observed in the exponential profile case.

Through spatio-temporal spectral analysis, each excited frequency can be related to an excited structural wavenumber. In the linear shear case, only high wavenumbers corresponding to three adjacent sine Fourier modes, $n \in \{13,14,15\}$ with the $n$th mode defined by $\sin(\pi n z D/L)$, are excited. In the exponential shear case, significant spectral contributions are noted at frequencies related to both high and low wavenumbers, corresponding to Fourier modes in the range

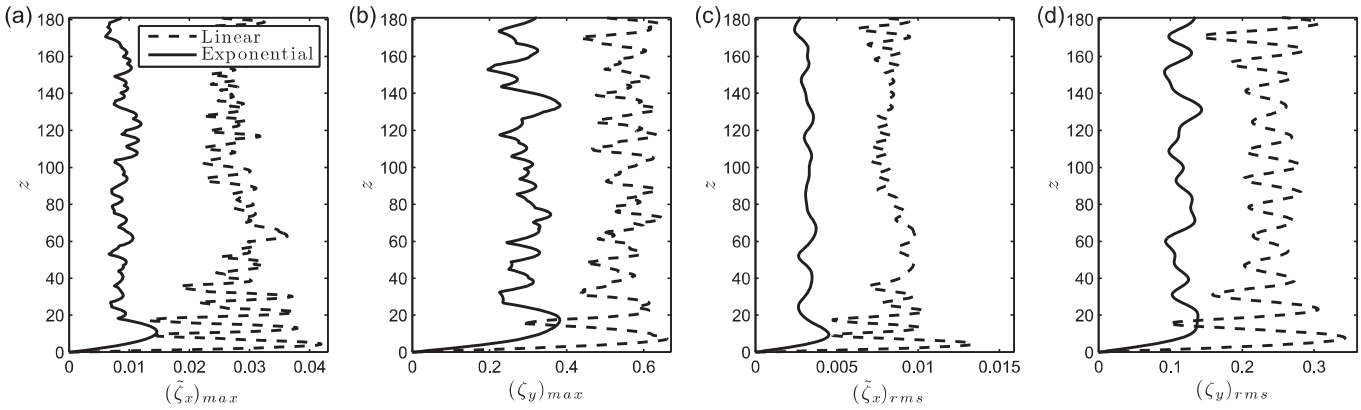


**Fig. 2.** (a, b) Maximum and (c, d) RMS values of the (a, c) in-line displacement fluctuation and (b, d) cross-flow displacement, along the span.

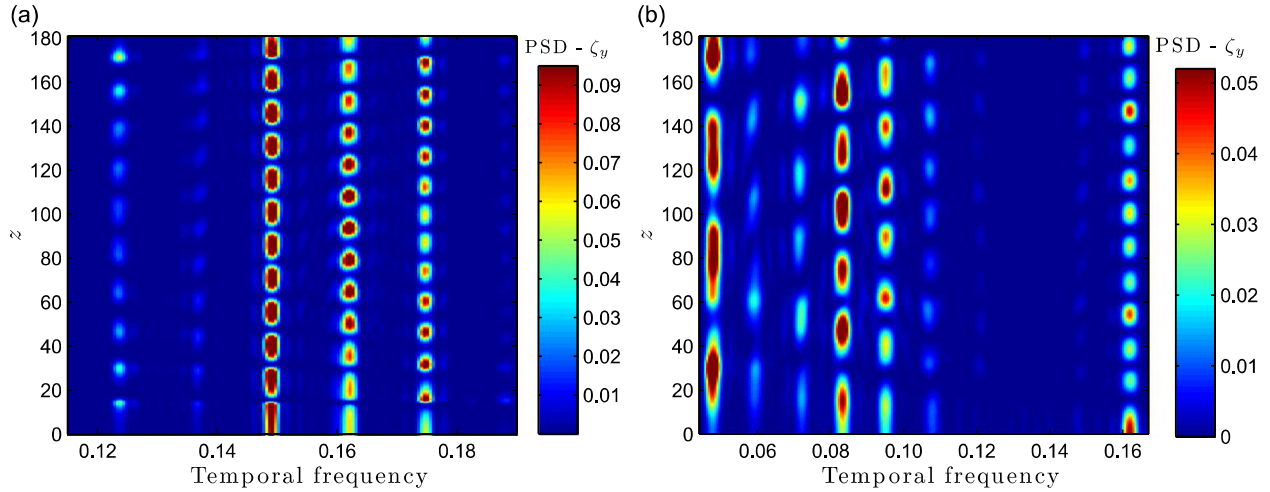


**Fig. 3.** PSD of the cross-flow displacement along the span for the (a) linear and (b) exponential inflow profiles. Selected natural frequencies of the structure are indicated by white dashed lines.

$n \in \{4,7,8,13\}$. The following dispersion relation may be used to estimate the natural frequency $f$ associated with the structural wavenumber $k$:

$$f = \sqrt{\frac{m}{m+\frac{\pi}{4}C_m}}k\sqrt{\omega_c^2+4\pi^2\omega_b^2k^2}, \tag{2}$$

where $C_m$ is the added mass coefficient induced by the fluid forces in phase with the beam acceleration. The natural frequencies associated with modes $11 \leq n \leq 15$ ($4 \leq n \leq 13$, respectively), for $C_m=1$, are indicated by white dashed lines in Fig. 3(a) (Fig. 3(b), respectively). The variability of the effective added mass coefficient can explain the deviations between the natural frequencies and the actual response peaks, as discussed in Section 5.

Similar observations can be made in the in-line direction where the structural response also exhibits a clear narrowband or broadband character, depending on the oncoming flow velocity profile. Each excited frequency in the cross-flow direction can be associated, with a ratio of 2, to an excited frequency in the in-line direction.

## 4. Impact of the shear profile on wake-body synchronization

The PSD of the cross-flow component of the flow velocity, $v$, in the wake, is used to identify the vortex shedding frequency along the span; the PSDs of $v$ associated with the linear and exponential inflow profiles are presented in Fig. 4(a) and (b). In these plots, the predominant cross-flow vibration frequencies, identified in Fig. 3, are indicated by white dashed lines. The lock-in condition is defined as the local synchronization between the vortex shedding and the cross-flow vibration; if the local vibration and vortex formation frequencies differ, the condition is referred to as non-lock-in. In the linear shear case, the lock-in condition occurs within a limited region on the high velocity side. The case of exponential shear exhibits a contrasted behavior: the lock-in condition is distributed along the length of the body and occurs both in the high and low flow velocity zones.

Under both the lock-in and non-lock-in conditions, vortex shedding occurs mainly at a single frequency at a given spanwise location, despite the multi-frequency nature of the vibrations. The wake-body synchronization is thus locally

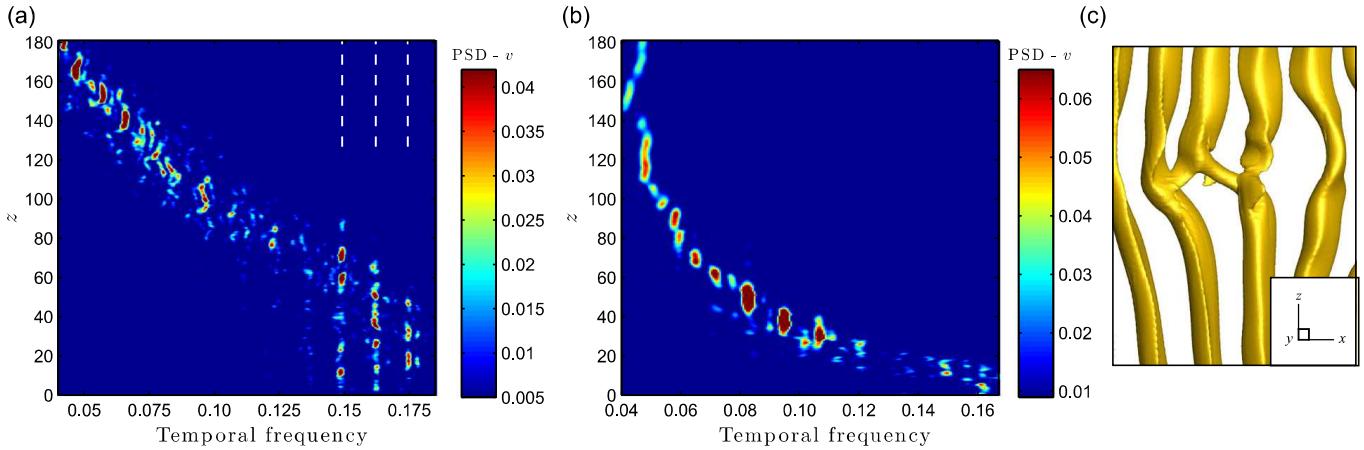


**Fig. 4.** (a, b) PSD of the cross-flow component of flow velocity along a spanwise line in the wake, for the (a) linear and (b) exponential inflow profiles. White dashed lines indicate the predominant frequencies of the cross-flow vibrations. (c) Instantaneous iso-surface of spanwise vorticity ($\omega_z = -0.03$) downstream of the beam ($(x,z) \in ([13,35] \times [140,175])$), in the exponential profile case.

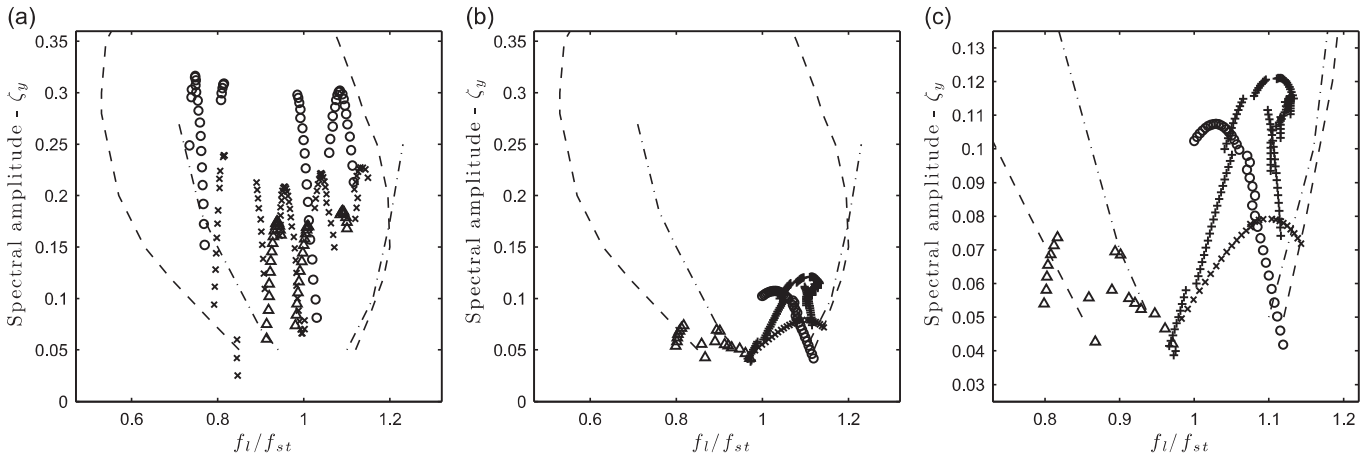


**Fig. 5.** Spectral amplitude of the cross-flow displacement under the lock-in condition as a function of the local vibration frequency normalized by the Strouhal frequency, for the (a) linear and (b) exponential inflow profiles. (c) Detailed view of (b). Different symbols are used to identify the lock-in frequency at each spanwise location: in (a) (○) $f$=0.149, (×) $f$=0.162, (△) $f$=0.174, in (b,c), (+) $f$=0.048, (○) $f$=0.083, (×) $f$=0.095, (△) $f$=0.162. The lower and upper limits of wake capture regions reported by Koopmann (1967) and Cheng and Moretti (1991), obtained through forced oscillation experiments, are indicated by dashed dotted and dashed lines, respectively.

mono-frequency. The spanwise discontinuities in the vortex shedding frequency are accompanied by vortex splittings that ensure the continuity of the vortex filaments between two adjacent cells, as illustrated in Fig. 4(c).

The spectral amplitude of the predominant component of the cross-flow vibration, locally involved in the lock-in condition, is plotted in Fig. 5, as a function of the local vibration frequency, $f_l$, normalized by the local Strouhal frequency, $f_{st}$, at the local Reynolds number (Williamson, 1996). The spanwise trend of the frequency of vortex formation globally follows the Strouhal law (Fig. 4(a) and (b)). However, under the lock-in condition, this frequency significantly shifts from the frequency of shedding downstream of a stationary cylinder, as can be observed in Fig. 5. Exceptions exist, but for both shear profiles the multi-frequency response amplitudes and associated lock-in frequencies generally remain within the wake capture region determined by Koopmann (1967) and Cheng and Moretti (1991) for forced cross-flow oscillations of a rigid cylinder in uniform current at $\mathrm{Re} \in \{100,200,300\}$ and $\mathrm{Re} = 1{,}500$, respectively, as also reported in the mono-frequency case (Bourguet et al., 2011a).

The impact of the shape of the inflow profile on the synchronization between the in-line and cross-flow vibrations can be monitored via the phase difference $\Phi_{xy} = [\phi_x - 2\phi_y, \mathrm{mod}\ 360^\circ]$, where the instantaneous phases of the in-line and cross-flow responses ($\phi_x$ and $\phi_y$, respectively) are determined by means of the Hilbert transform. For mono-frequency VIV of long flexible cylinders in shear flow, the lock-in condition occurs mainly through counter-clockwise figure eight orbits, in which the body moves upstream at the extremes of the cross-flow motion (Bourguet et al., 2011c; Modarres-Sadeghi et al., 2010; Vandiver et al., 2009). In the case of mono-frequency responses, the cylinder describes counter-clockwise orbits for $\Phi_{xy}$ in the range 0°–180°, and clockwise orbits for $\Phi_{xy}$ in the range 180°–360°. Typical trajectories observed in the present narrowband response case (linear shear) resemble mono-frequency VIV figure eight orbits, as illustrated in Fig. 6(a).

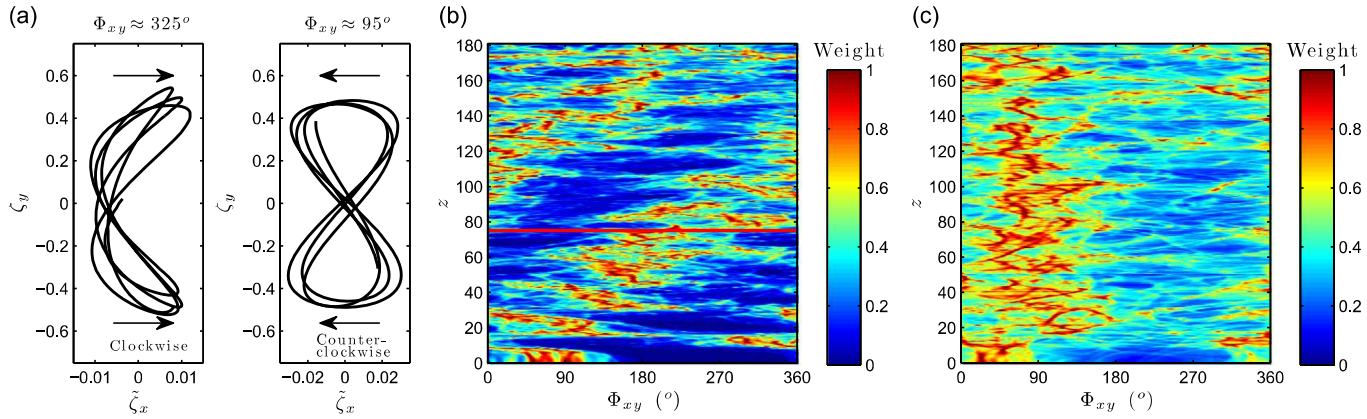


**Fig. 6.** (a) Selected trajectories of the beam resembling clockwise ($z=10.5$) and counter-clockwise ($z=5.5$) figure-eight orbits, in the case of narrowband responses (linear inflow profile). (b, c) Histogram of phase difference between the in-line and cross-flow displacements along the span for the (b) linear and (c) exponential inflow profiles. In (b, c), the limit between counter-clockwise and clockwise orbits in the case of mono-frequency responses ($\Phi_{xy} = 180^\circ$) is indicated by a white vertical dashed line. In (b), a red horizontal plain line denotes the limit of the lock-in region. (For interpretation of the references to color in this figure caption, the reader is referred to the web version of this paper.)

The histograms of $\Phi_{xy}$ determined from the entire time series of displacements are plotted along the span for the linear and exponential inflow profiles in Fig. 6(b) and (c).

As reported in a previous work (Bourguet et al., 2012), the narrowband response case exhibits a synchronization pattern similar to the mono-frequency case, with mainly counter-clockwise orbits in the region of lock-in (identified by a red horizontal line in Fig. 6(b)), and a clear spanwise drift of the phase difference. In the exponential shear case (broadband responses), the beam orbits do not generally resemble figure-eight trajectories. Despite noisier histograms, a synchronization pattern exists between the in-line and cross-flow vibrations and $\Phi_{xy}$ remains generally lower than 180° along the span. Hence, the in-line and cross-flow vibrations appear to be locked to a specific phase difference range and no drift can be identified along the beam.

## 5. Fluid forces in narrowband and broadband VIV cases

The spatio-temporal evolutions of the fluid forces in both shear profile cases are illustrated in Fig. 7(a) and (b) by selected time series of the cross-flow force normalized using the local inflow velocity $U_l$, $C_l = C_y U^2 / U_l^2$. The present analysis focuses on the cross-flow force; similar features can be noted in the in-line direction. In spite of the change in the nature of the structural responses due to the modification of the shear profile, both cases exhibit comparable standing-traveling wave patterns of the force coefficient. The spanwise evolution of the temporal PSD of $C_l$ is plotted in Fig. 7(c) and (d), for both current profiles. The main components of the force generally peak at the predominant vibration frequencies, indicated by white dashed lines in these plots. The three components associated with the three high-wavenumber vibration frequencies in the narrowband case (linear shear) present spectral contributions of similar magnitudes over a wide portion of the beam. In the broadband response case (exponential shear), the high frequency component dominates the force spectrum while the three other vibration frequencies, related to lower spatial wavenumbers, present secondary contributions. This behavior contrasts with the cross-flow displacement PSD (Fig. 3(b)) and explains the similarity noted in the spatio-temporal patterns of the fluid force between the two sheared current cases while the vibration patterns substantially differ.

Another feature can be identified for the exponential shear case: at each spanwise location, the fluid force exhibits significant spectral amplitudes only at vibration frequencies equal to or higher than the local shedding frequency. This phenomenon cannot be established in the narrowband response case due to the proximity of the excited frequencies, and to the interwoven distribution of the lock-in cells, whose respective frequencies do not decrease monotonically along the span as in the case of broadband VIV.

The time-averaged values of the in-line force coefficient and the maximum and RMS values of the in-line and cross-flow force coefficients are presented in Fig. 8, for both inflow profiles. In these plots, the force normalization is based on the local inflow velocity. The force coefficients reach high magnitudes compared to the values reported for a stationary cylinder (e.g. Norberg, 2003; Persillon and Braza, 1998). Previous studies concerning oscillating rigid cylinders have emphasized the impact of the cross-flow vibration amplitude on the in-line forces (Bishop and Hassan, 1964; Carberry et al., 2005; Khalak and Williamson, 1999). Hence, the observed amplification of the mean and fluctuating in-line force coefficients between the exponential and linear inflow cases can be related to the increased vibration amplitudes in the latter case. In addition, larger deviations of the maximum and RMS values of this coefficient between the two cases can be noted on the low velocity side, for $z > 110$ approximately. Such divergence may be associated with the occurrence of the lock-in condition in this region, in the exponential shear case, while in the linear shear case, vortex formation and beam oscillation are not synchronized in this area. For both current profiles, the cross-flow force coefficients present very similar

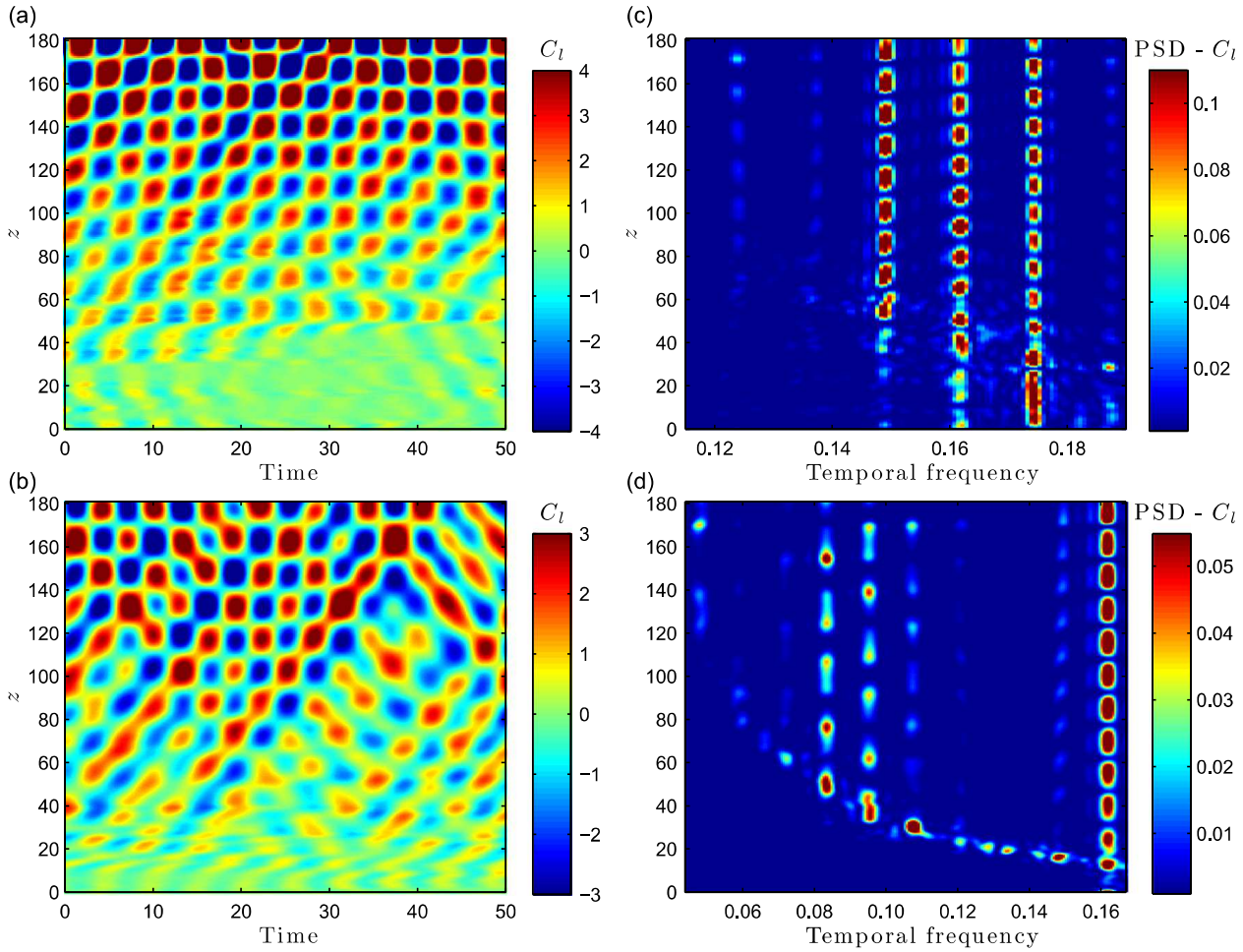


**Fig. 7.** (a, b) Selected time series and (c, d) PSD of the cross-flow force coefficient along the span, for the (a, c) linear and (b, d) exponential inflow profiles. The force normalization is based on the local inflow velocity. In (c, d), white dashed lines indicate the predominant frequencies of the cross-flow vibrations.

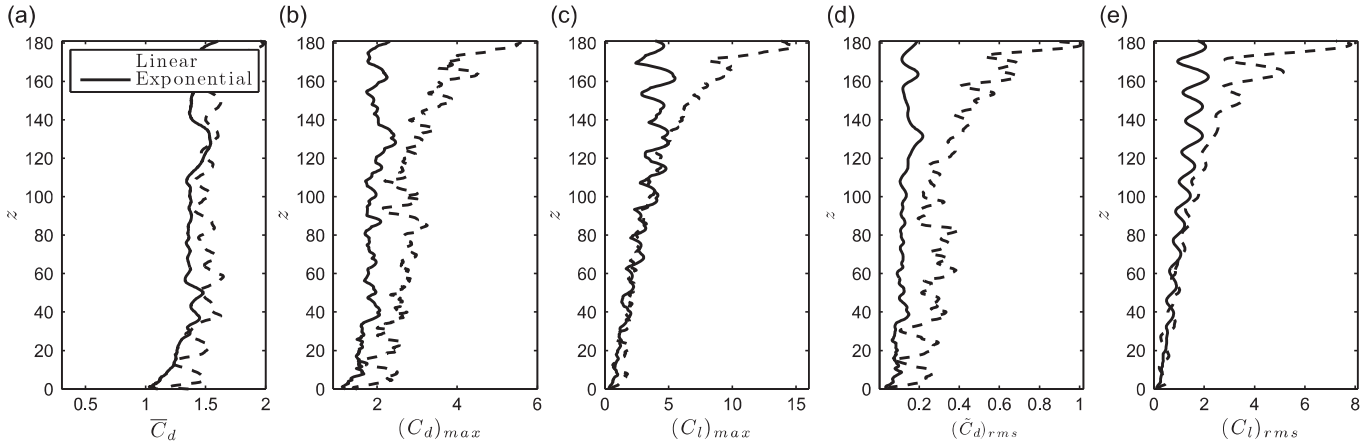


**Fig. 8.** (a) Time-averaged in-line force coefficient, (b, c) maximum and (d, e) RMS values of the (b, d) in-line and (c, e) cross-flow force coefficients, along the span. In (d), the deviation of the in-line force coefficient from its time-averaged value, $\tilde{C}_d$, is considered. The force normalization is based on the local inflow velocity.

trends over a portion of the span. However, considerable differences can be noted on the low velocity side as the cross-flow force also appears to be impacted by the occurrence of the lock-in or non-lock-in condition in this region, depending on the shear profile.

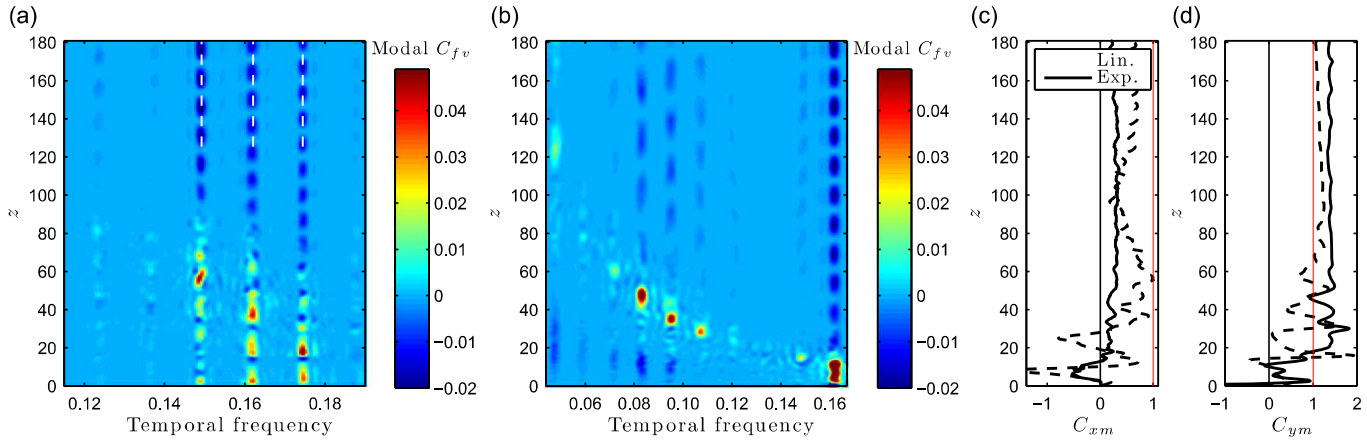


**Fig. 9.** (a, b) Frequency decomposition of the force coefficient in phase with the beam velocity for the (a) linear and (b) exponential inflow profiles, along the span. White dashed lines indicate the predominant frequencies of the cross-flow vibrations. Effective (c) in-line and (d) cross-flow added mass coefficients along the span. In (c, d), the potential flow value of 1 is indicated by a red plain line. (For interpretation of the references to color in this figure caption, the reader is referred to the web version of this paper.)

The fluid force coefficient in phase with the body velocity, including the in-line and cross-flow contributions, is used to monitor the energy transfer between the flow and the vibrating structure

$$C_{fv} = \frac{\sqrt{2}\left\langle \tilde{C}_x \frac{\partial \tilde{\zeta}_x}{\partial t} + C_y \frac{\partial \zeta_y}{\partial t} \right\rangle}{\sqrt{\left\langle \left(\frac{\partial \tilde{\zeta}_x}{\partial t}\right)^2 + \left(\frac{\partial \zeta_y}{\partial t}\right)^2 \right\rangle}}, \tag{3}$$

where $\langle \cdot \rangle$ denotes the time-averaging operator and $\tilde{C}_x$ is the fluctuating component of $C_x$. A frequency decomposition of $C_{fv}$ is plotted along the span for each current profile in Fig. 9(a) and (b). Positive energy transfer from the fluid to the structure ($C_{fv} > 0$), i.e. structure excitation by the flow, occurs locally under the lock-in condition; the non-lock-in condition is associated with damping fluid forces ($C_{fv} < 0$). For both inflow velocity profiles, wake-body synchronization is generally established at a single frequency at a given spanwise location; therefore, the structure excitation is locally mono-frequency. The narrowband response case exhibits a well-defined spanwise pattern composed of a zone of excitation located in the high velocity region and a zone of vibration damping located on the low velocity side. In contrast, excitation regions are distributed along the span in the case of broadband vibrations. It appears that small positive values of $C_{fv}$ can lead to significant structural responses as illustrated by the low-frequency component of the vibration in the exponential shear case ($f$=0.048, Fig. 9(b)).

The effective in-line and cross-flow added mass coefficients due to the fluid forces in phase with the beam acceleration are determined as follows:

$$C_{xm} = -\frac{2}{\pi} \frac{\left\langle \tilde{C}_x \frac{\partial^2 \tilde{\zeta}_x}{\partial t^2} \right\rangle}{\left\langle \left(\frac{\partial^2 \tilde{\zeta}_x}{\partial t^2}\right)^2 \right\rangle}, \quad C_{ym} = -\frac{2}{\pi} \frac{\left\langle C_y \frac{\partial^2 \zeta_y}{\partial t^2} \right\rangle}{\left\langle \left(\frac{\partial^2 \zeta_y}{\partial t^2}\right)^2 \right\rangle}. \tag{4}$$

As can be observed in Fig. 9(c) and (d), $C_{xm}$ and $C_{ym}$ present large spanwise modulations, especially within the high velocity zone which corresponds in both cases to regions of lock-in at high or intermediate frequencies. Such variability of the effective added mass coefficient induces deviations from the dispersion relation (2), where the added mass is assumed to be constant along the span. Smoother trends are noted along the rest of the span, but the added mass values can differ substantially from the potential flow value of 1; the departure from 1 is generally larger in the exponential shear case.

## 6. Conclusions

The VIV of a long cylindrical tensioned beam immersed in linearly and exponentially sheared currents have been analyzed by means of direct numerical simulation, with an emphasis on the impact of the shape of the inflow profile on the fluid–structure interaction mechanisms.

Both inflow profile shapes excite responses at multiple frequencies, but the structural vibrations differ substantially in their spectral content: narrowband, high-wavenumber vibrations are noted in the linear shear case, while broadband vibrations, involving a wide range of excited frequencies and spatial wavenumbers, appear in the exponential case. For both shear profiles, mixed standing-traveling wave responses of the flexible body are excited under the lock-in condition.

In the linear shear case, narrowband response excitation occurs within a limited region of the high inflow velocity zone, while the broadband vibrations observed in the exponential shear flow are excited in several regions of the beam, through a distributed occurrence of the lock-in condition.

The switch from narrowband to broadband VIV, as the current profile is modified, is accompanied by an alteration of the synchronization pattern between the in-line and cross-flow responses. Drifting phase difference and preferential occurrence of counter-clockwise figure-eight orbits in the lock-in region are noted in the narrowband case, which are similar to those reported for mono-frequency vibrations. In contrast, the in-line and cross-flow broadband responses of the exponential inflow profile appear to be phase-locked and no phase drift can be identified along the beam span.

For both the in-line and cross-flow directions, the case of exponential shear presents lower vibration amplitudes. This change can be related to the observed decrease in the time-averaged and fluctuating in-line forces between narrowband and broadband vibrations. The cross-flow force exhibits similar behavior in both cases, except in zones where the lock-in condition is established in the broadband case but not in the narrowband case; diverging trends are noted in these zones, for both the in-line and cross-flow forces. Despite a considerable modification of the vibration spectral content, the forces present qualitatively comparable spatio-temporal patterns for both current profiles. This is due to the predominant contribution of the high-frequency components in the broadband case. The variability of the effective added mass coefficients, noted in both cases, contributes to the observed departure of the excited vibration frequencies from those predicted by the tensioned beam dispersion relation.

## Acknowledgments

The authors wish to acknowledge support from the BP-MIT Major Projects Programme, monitored by M. Tognarelli and P. Beynet; and the Office of Naval Research under Grants N00014-07-1-0135 and N00014-07-1-0446, monitored by T. Swean, Jr.

## References

Bearman, P.W., 1984. Vortex shedding from oscillating bluff bodies. Annual Review of Fluid Mechanics 16, 195–222.
Bearman, P.W., 2011. Circular cylinder wakes and vortex-induced vibrations. Journal of Fluids and Structures 27, 648–658.
Bishop, R.E.D., Hassan, A.Y., 1964. The lift and drag forces on a circular cylinder oscillating in a flowing fluid. Proceedings of the Royal Society of London. Series A, Mathematical and Physical Sciences 277, 51–75.
Bourguet, R., Karniadakis, G.E., Triantafyllou, M.S., 2011a. Lock-in of the vortex-induced vibrations of a long tensioned beam in shear flow. Journal of Fluids and Structures 27, 838–847.
Bourguet, R., Karniadakis, G.E., Triantafyllou, M.S., 2011b. Vortex-induced vibrations of a long flexible cylinder in shear flow. Journal of Fluid Mechanics 677, 342–382.
Bourguet, R., Modarres-Sadeghi, Y., Karniadakis, G.E., Triantafyllou, M.S., 2011c. Wake-body resonance of long flexible structures is dominated by counter-clockwise orbits. Physical Review Letters 107, 134502.
Bourguet, R., Lucor, D., Triantafyllou, M.S., 2012. Mono- and multi-frequency vortex-induced vibrations of a long tensioned beam in shear flow. Journal of Fluids and Structures 32, 52–64.
Carberry, J., Sheridan, J., Rockwell, D., 2005. Controlled oscillations of a cylinder: forces and wake modes. Journal of Fluid Mechanics 538, 31–69.
Chaplin, J.R., Bearman, P.W., Huera-Huarte, F.J., Pattenden, R.J., 2005. Laboratory measurements of vortex-induced vibrations of a vertical tension riser in a stepped current. Journal of Fluids and Structures 21, 3–24.
Cheng, M., Moretti, P.M., 1991. Lock-in phenomena on a single cylinder with forced transverse vibration. In: Flow-Induced Vibration and Wear, ASME PVP, vol. 206, pp. 129–133.
Dahl, J.M., Hover, F.S., Triantafyllou, M.S., Oakley, O.H., 2010. Dual resonance in vortex-induced vibrations at subcritical and supercritical Reynolds numbers. Journal of Fluid Mechanics 643, 395–424.
Evangelinos, C., Karniadakis, G.E., 1999. Dynamics and flow structures in the turbulent wake of rigid and flexible cylinders subject to vortex-induced vibrations. Journal of Fluid Mechanics 400, 91–124.
Huera-Huarte, F.J., Bearman, P.W., 2009. Wake structures and vortex-induced vibrations of a long flexible cylinder part 1: dynamic response. Journal of Fluids and Structures 25, 969–990.
Karniadakis, G.E., Sherwin, S., 1999. Spectral/hp Element Methods for CFD, 1st ed. Oxford University Press, Oxford.
Khalak, A., Williamson, C.H.K., 1999. Motions, forces and mode transitions in vortex-induced vibrations at low mass-damping. Journal of Fluids and Structures 13, 813–851.
Koopmann, G.H., 1967. The vortex wakes of vibrating cylinders at low reynolds numbers. Journal of Fluid Mechanics 28, 501–512.
Lie, H., Kaasen, K.E., 2006. Modal analysis of measurements from a large-scale VIV model test of a riser in linearly sheared flow. Journal of Fluids and Structures 22, 557–575.
Lucor, D., Imas, L., Karniadakis, G.E., 2001. Vortex dislocations and force distribution of long flexible cylinders subjected to sheared flows. Journal of Fluids and Structures 15, 641–650.
Lucor, D., Mukundan, H., Triantafyllou, M.S., 2006. Riser modal identification in CFD and full-scale experiments. Journal of Fluids and Structures 22, 905–917.
Modarres-Sadeghi, Y., Mukundan, H., Dahl, J.M., Hover, F.S., Triantafyllou, M.S., 2010. The effect of higher harmonic forces on fatigue life of marine risers. Journal of Sound and Vibration 329, 43–55.
Newman, D.J., Karniadakis, G.E., 1997. A direct numerical simulation study of flow past a freely vibrating cable. Journal of Fluid Mechanics 344, 95–136.
Norberg, C., 2003. Fluctuating lift on a circular cylinder: review and new measurements. Journal of Fluids and Structures 17, 57–96.
Persillon, H., Braza, M., 1998. Physical analysis of the transition to turbulence in the wake of a circular cylinder by three-dimensional Navier–Stokes simulation. Journal of Fluid Mechanics 365, 23–88.
Prasanth, T.K., Mittal, S., 2008. Vortex-induced vibrations of a circular cylinder at low Reynolds numbers. Journal of Fluid Mechanics 594, 463–491.
Sarpkaya, T., 2004. A critical review of the intrinsic nature of vortex-induced vibrations. Journal of Fluids and Structures 19, 389–447.
Singh, S.P., Mittal, S., 2005. Vortex-induced oscillations at low reynolds numbers: hysteresis and vortex-shedding modes. Journal of Fluids and Structures 20, 1085–1104.

Trim, A.D., Braaten, H., Lie, H., Tognarelli, M.A., 2005. Experimental investigation of vortex-induced vibration of long marine risers. Journal of Fluids and Structures 21, 335–361.
Vandiver, J.K., Allen, D., Li, L., 1996. The occurrence of lock-in under highly sheared conditions. Journal of Fluids and Structures 10, 555–561.
Vandiver, J.K., Jaiswal, V., Jhingran, V., 2009. Insights on vortex-induced, traveling waves on long risers. Journal of Fluids and Structures 25, 641–653.
Williamson, C.H.K., 1996. Vortex dynamics in the cylinder wake. Annual Review of Fluid Mechanics 28, 477–539.
Williamson, C.H.K., Govardhan, R., 2004. Vortex-induced vibrations. Annual Review of Fluid Mechanics 36, 413–455.